Numerical study of laminar magneto-convection in a differentially heated square duct

Numerical study of laminar magneto-convection in a differentially heated square duct

A Tassone, F Giannetti and G Caruso

Department of Astronautical, Electrical and Energy Engineering – Nuclear Section, Sapienza, Università di Roma, Corso Vittorio Emanuele II 244, Roma, Italy, 00186

Corresponding author: alessandro.tassone@uniroma1.it

Abstract Magnetohydrodynamic pressure drops are one of the main issues for liquid metal blanket in fusion reactors. Minimize the fluid velocity at few millimeters per second is one strategy that can be employed to address the problem. For such low velocities, buoyant forces can effectively contribute to drive the flow and therefore must be considered in the blanket design. In order to do so, a CFD code able to represent magneto-convective phenomena is required. This work aims to gauge the capability of ANSYS© CFX-15 to solve such cases. The laminar flow in a differentially heated duct was selected as validation benchmark. A horizontal and uniform magnetic field was imposed over a square duct with a linear and constant temperature gradient perpendicular to the field. The fully developed flow was analyzed for $Gr = 10^5$ and Hartmann number (M) ranging from 10^2 to 10^3. Both insulating and conducting duct walls were considered. Strong dampening of the flow in the center of the duct was observed, whereas high velocity jets appeared close to the walls parallel to the magnetic field. The numerical results were validated against theoretical and numerical results founding an excellent agreement.

1. Introduction

Liquid metals are often considered as the working fluid for tokamak fusion reactors thanks to their excellent thermo-hydraulics and tritium breeding properties. The eutectic alloy of lithium and lead (LiPb) is the leading candidate and it is actually being studied in three out of the four blanket concepts considered for the PPPT EUROfusion Breeding Blanket project. Although attractive, LiPb has many issues still to be addressed. One of the most important is the interaction between the fluid and the containment magnetic field which sensibly modifies the features of the flow inside the blanket, i.e. electromagnetic drag, enhanced corrosion rate, turbulence suppression, etc. [1]. In order to reduce the MHD contribution to the pressure drops, the molten metal can be employed exclusively as a tritium breeder, whereas the role of coolant for the blanket and the first wall is assumed by a non-conductive fluid, usually water or helium. In this configuration, the liquid metal velocity is reduced to a few millimeters per second and therefore the MHD pressure drops are greatly limited. However, for such low velocities, the buoyancy forces arising from the temperature distribution inside the fluid can play an important role and thus the phenomenon of magneto-convection must be considered during the design of the blanket.

One of the most studied case, both theoretically [2][3][4] and experimentally [5][6], is the buoyant flow which arises in a differentially heated vertical duct when a strong transverse magnetic field is applied. Similar geometries are often encountered in helium-cooled blankets. To support the blanket design, a

CFD code able to tackle the complexity of MHD problems for the values of the fundamental parameters expected is required. Despite the many efforts of the fusion community spent in the development, a mature code specifically tailored to simulate MHD flows is still unavailable. Main-purpose codes are often employed to realize MHD analyses, using available built-in models (which usually require an additional license) or modifying the governing equations of the ordinary hydrodynamic flow [7]. In the past, a user-modified version of ANSYS CFX was studied and found to represent successfully the main features of MHD buoyant flows [8]. Since 2009, a MHD module has been available as an add-on of the main code and this paper aims to assess the capability of ANSYS© CFX-15 to reproduce the phenomena of magneto-convection.

2. Formulation

In this section the governing equations of the MHD flow will be outlined following the ϕ-formulation employed by the CFX solver [9]. A sketch of the problem geometry is provided in Figure 1a.
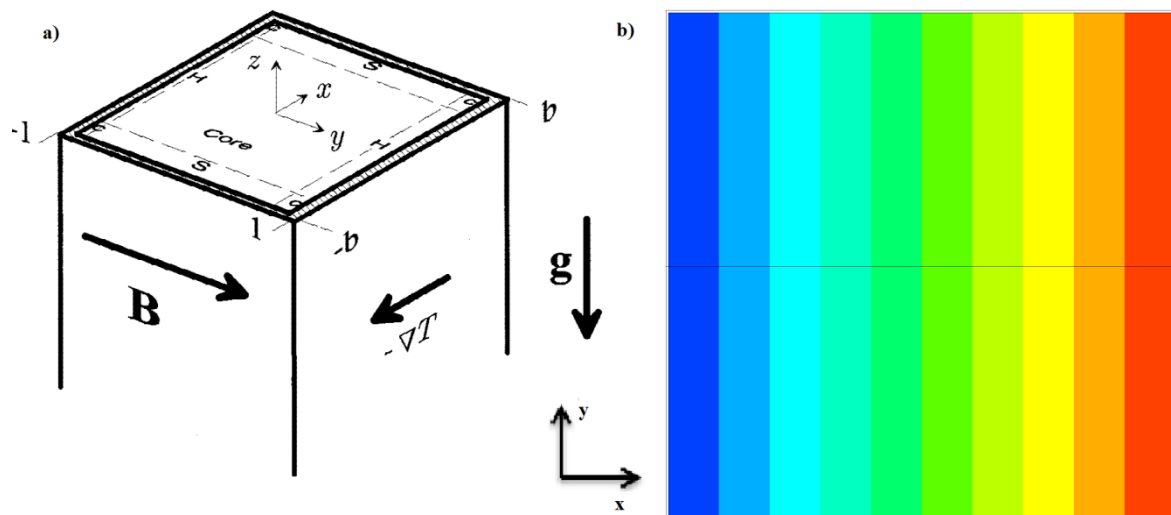
Figure 1 a) Sketch of the benchmark geometry [8] (left), **b)** Temperature contour (right)

The duct is filled with LiPb, initially at rest. Two opposite walls of the duct are kept at fixed temperature values, whereas the other duct walls are assumed as adiabatic. A constant temperature gradient $\nabla \boldsymbol{T} = \hat{x}$ is considered as the source of momentum for the fluid. A uniform and constant transverse magnetic field $\boldsymbol{B} = \hat{y}$, perpendicular to the temperature gradient, is applied. The pair of walls parallel to the magnetic field are called *side walls*, whereas the pair orthogonal to it are called *Hartmann walls*. The gravitational acceleration $\boldsymbol{g} = -\hat{z}$ is aligned with the duct axis. The physical proprieties of the fluid are assumed constant in the range of temperature considered and evaluated at the reference temperature T_0. The only exception to this assumption is the density in the gravitational body force term which, employing the Boussinesq approximation, it is a linear function of the temperature. Since the fluid considered is LiPb, which is characterized by a low value of the magnetic Reynolds number ($R_m \ll 1$), the induction-less approximation can be employed and then the induced magnetic field neglected [10]. Under these conditions, a steady flow would be governed by the non-dimensional MHD momentum equation

$$\frac{Gr}{M^4}(\boldsymbol{v} \cdot \boldsymbol{\nabla})\boldsymbol{v} = -\nabla p + \frac{1}{M^2}\nabla^2 \boldsymbol{v} + \boldsymbol{j} \times \boldsymbol{B} + T\hat{x}$$

(1)

and the continuity equation

$$\nabla \cdot \boldsymbol{v} = 0$$

(2)

The vectors $\boldsymbol{v}$ and $\boldsymbol{j}$ are the fluid velocity and the electric current density. These quantities would be scaled respectively with $w_0 = \nu Gr/L\,M^2$ and $j_0 = \sigma w_0 B$ where ν is the fluid kinematic viscosity and σ the electrical conductivity. The symbols Gr and M identify the non-dimensional parameters *Grashof number* and *Hartmann number*. The former quantifies the intensity of the buoyancy forces compared with the viscous forces in the fluid, whereas the latter is correlated to the ratio between the electromagnetic forces and the viscous forces. They are expressed with the relations

$$Gr = g\beta\,\Delta T\,L^3/\nu^2 \tag{3}$$

$$M = BL\sqrt{\sigma/\rho\nu} \tag{4}$$

where β is the thermal expansion coefficient, ΔT is a characteristic temperature difference and L is the length scale of the flow, usually the half-width of the duct in the direction of the magnetic field. The ratio Gr/M^2 which appears in the velocity scale can be considered as an analogue of the Reynolds number, whereas the ratio Gr/M^4 is the buoyant MHD equivalent of the interaction parameter N. The temperature T is the difference between the local and the reference temperature T_0 divided by ΔT. The scaled pressure p is the difference between the local and the hydrostatic pressure evaluated at T_0 divided by $\sigma w_0 B^2 L$. The electric current density is obtained by the Ohm's law and the charge conservation

$$\boldsymbol{j} = -\nabla\phi + \boldsymbol{v}\times\boldsymbol{B} \tag{5}$$

$$\nabla\cdot\boldsymbol{j} = 0 \tag{6}$$

where ϕ is the electric potential, which is scaled by $Lw_0 B$. Combining (5) and (6), a Poisson equation for the potential is obtained that, once resolved, gives the distribution of the electric potential and then the one of the current density

$$\nabla^2\phi = \nabla\cdot(\boldsymbol{v}\times\boldsymbol{B}) \tag{7}$$

The temperature distribution will be obtained by the non-dimensional energy equation

$$Pe(\boldsymbol{v}\cdot\nabla)\boldsymbol{T} = \nabla^2\boldsymbol{T} + Q \tag{8}$$

where $Pe = Gr\,Pr/M^2$ is the Peclet number and Q is the non-dimensional volumetric heat source term. Since the fluid is a liquid metal ($Pr \ll 1$), for a laminar flow the condition $Pe \ll 1$ is satisfied and then the distribution of temperature is independent by the velocity field **(Figure 1b)**. In the following, the source term Q will be considered as negligible. Then, Eq. (8) will reduce to a Laplace equation, the solution of which will be a linear temperature distribution [3]. The flow features are affected by the duct walls electric conductivity, which is assumed to have an arbitrary value. To denote that, the parameter wall conductance ratio is introduced with the following expression

$$c = (\sigma_w t)/(\sigma L) \tag{9}$$

The symbol σ_w identifies the wall electrical conductivity and t the wall thickness. In the following it will arise the necessity to distinguish between the conductance ratio of the side walls (c_S) and of the Hartmann walls (c_H).

3. Numerical strategy
The dimensionless parameters considered for the study are available in Table 1. Two coupled computational domains (one for the LiPb, the other for the walls) were employed. The fluid properties

were evaluated at $T_0 = 600\ K$ and according to the correlations available in [11]. A linear temperature profile was deduced from the simplified expression of (8) and imposed on both the domains through the setup of fixed temperature boundary conditions on the duct walls parallel to the x-axis. For the other walls the adiabatic boundary condition ($\partial T_n = 0$) was assumed. Therefore, a purely conductive heat transfer regime is established in the duct. Eq. (1), (2) and (7) are solved by CFX in the fluid domain, whereas just Eq. (1) and (7) are considered in the solid one. The code results were validated employing the analytical solutions developed in [3]. These were obtained with an asymptotic analysis for a fully developed flow that, therefore, must satisfy the conditions

$$Gr/M^4 \ll 1 \qquad\qquad (10)$$
$$c_S \gg M^{-\frac{1}{2}} \qquad\qquad (11)$$

The inertia-less condition (10) is satisfied for a sufficiently long duct. Since Eq. (11) requires that no currents close through the side wall boundary layers, thus ruling out the limiting case of perfectly insulating walls ($c = 0$), for these cases the numerical results presented in [8] and [12] were used for validation purpose.

Table 1 Dimensionless groups

Gr	Pr	Pe	M	c
		$2.68 \cdot 10^{-1}$	10^2	0
				∞
10^5	$2.68 \cdot 10^{-2}$	$1.67 \cdot 10^{-2}$	$4 \cdot 10^2$	0
				∞
		$2.68 \cdot 10^{-3}$	10^3	0
				∞

The quality of the numerical results was gauged with two indices: a local error, using as reference the flow peak velocity, and an integral error, evaluated with the root squared deviation from the analytical value of the integral of the velocity profile. For the latter, the velocity profile plotted at $y = 0$ was considered. For the integral error a maximum value of 2% was deemed acceptable, whereas for the peak this condition was relaxed to 5%. The fully developed flow profile was obtained by rendering only a tiny slice of the duct and imposing periodic boundary conditions for all the variables on the top and bottom surfaces, thus simulating an infinitely tall duct with a small computational effort. The no-slip boundary condition was applied at the walls for the velocity, together with the conservation of potential and current density. At the external wall surface, a zero-flux boundary condition for J was imposed to satisfy Eq. (6). For each M, test cases with perfectly conducting ($c = \infty$) and insulating walls were performed. Moreover, for $M = 10^2$, simulations with wall conductance ratio ranging from $c = 1$ to $c = 10^{-3}$ were realized in order to test the capability of the code in dealing with finite wall conductivity flows.

3.1. Computational grid
Due to the presence of the magnetic field, the boundary layers of a MHD flow have a different behavior depending on the relative orientation between the wall and the field. For a Hartmann wall, the layer thickness is calculated with the scaling law $\delta_H = 1/M$, whereas for a side wall the law $\delta_S = 1/\sqrt{M}$ is valid. This difference of scale has been addressed by the benchmark mesh employing custom inflation settings. Since it is characterized by a steep velocity gradient, a sufficient number of nodes in the Hartmann layer are necessary to properly render the profile and avoid the under-estimation of the core velocity. A minimum of 3 nodes is required for the perfectly conducting case, whereas more points

would be needed for the finite conductivity and insulating cases in which the currents close through the layer. For this reason, all the benchmark simulations were performed with a mesh provided with 15 nodes in the Hartmann layer region. Outside of this tiny region, no significant change of the flow variables is expected along the magnetic field lines, therefore only 35 nodes are employed here. A different treatment must be applied in the direction perpendicular to the magnetic field where many more nodes are needed to follow the velocity and electric potential profile. In Figure 2, it can be seen the comparison of the results obtained by three grids of increasing resolution.

Side nodes	Peak Error	Integral Error
250	10.69%	10.78%
500	5.38%	5.35%
1000	2.20%	1.46%
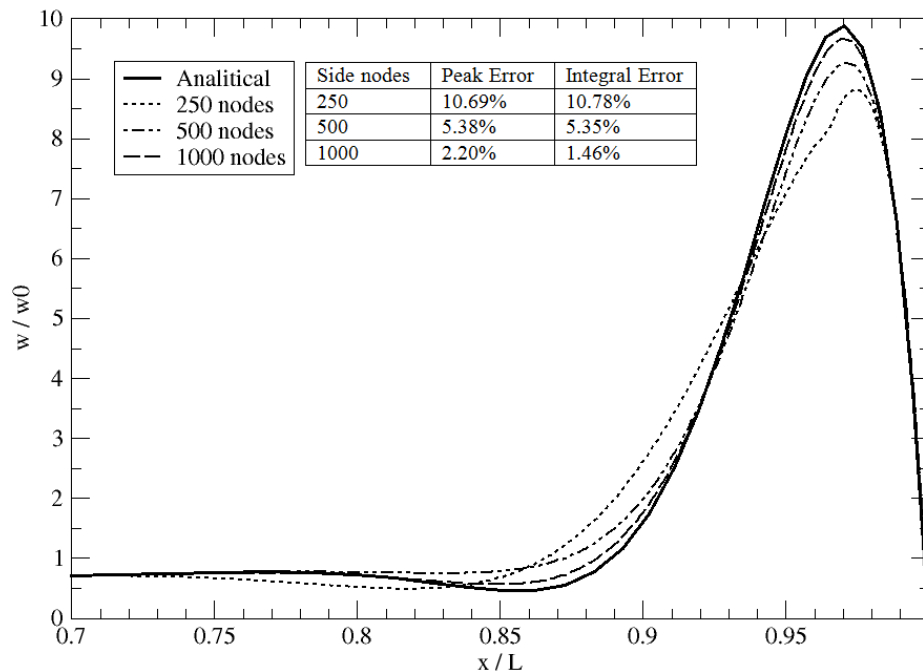
Figure 2 Grid sensitivity analysis for the side wall velocity profile at $y = 0$ for the $c = \infty$ and $M = 10^3$ case

The number of nodes needed for a constant accuracy increases with the Hartmann number: for the $M = 10^2$ test case, one hundred nodes on the half-width of the duct were sufficient to meet the peak error criterion, whereas for the $M = 1000$ case this number jumped to one thousand.

The benchmark is a 2D MHD flow case, since the induced currents are confined in the cross-section plane. Unlike other CFD codes as FLUENT or OpenFOAM, it is not possible to run a 2D simulation in CFX therefore a certain number of "useless" nodes must be allocated in the axial direction. To avoid the arise of numerical instability a minimum of 4 nodes are usually enough but, especially for high values of M, more nodes can be useful to foster the convergence and prevent "phantom" axial currents to appear. In order to proper satisfy the conservation of charge, a conformal mesh between the solid and the liquid computational domain was realized. The only exception was represented by the perfectly insulating case mesh where, since no current closes through the walls, the solid domain was not rendered.

All the simulations were performed with the "high resolution" advection scheme which is a local-weighted version of the upwind discretization scheme [10]. During the performing of the benchmark simulations it became clear that not all the methods provided by CFX for the calculation of the time-step are equally suitable for MHD purposes. In particular, the Local Timescale option, although the most robust, has been incapable to obtain the expected electric potential distribution and was prone to produce unphysical results. This difficulty was often overcome by performing a first run employing the Auto Timescale option to produce a distribution to use as an initial condition for the Local Timescale run which was then able to reach a meaningful solution.

4. Results and discussion

No driving pressure gradient was considered; the motion of the flow was sustained completely by buoyancy forces arising from the temperature distribution inside the duct, i.e. a linear profile $\boldsymbol{T} = T(x)\hat{\boldsymbol{x}}$ with the limiting values $T(-b) = -1$ and $T(b) = +1$.
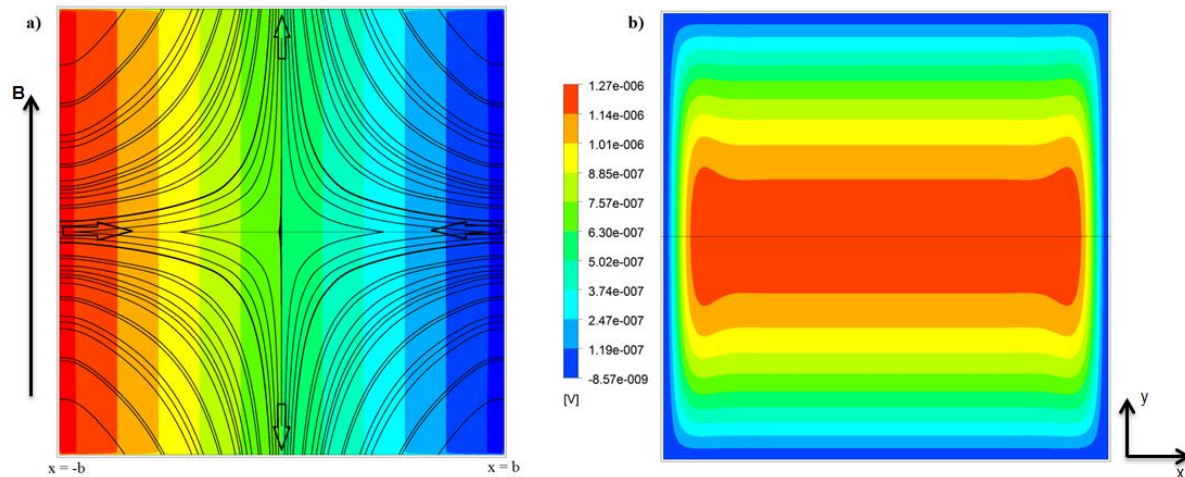
Figure 3 a) Electric current paths and Lorentz force contour (left), **b)** Electric potential contour for $\boldsymbol{c} = \infty$ (right)

4.1. Perfectly conducting walls

A single circulation cell appears with a rising jet near the hot wall and a descending one close to the cold wall. The flow is symmetric across the center line of the duct and the profile velocity is flattened in the core. An inflection point is present where the linear core profile meets the jet. Electric currents are induced in the core region of the duct. Since the conductivity of the side wall is much higher than the conductivity of the side walls boundary layer (11), the current pass through the latter and close in the former. In Figure 3a the current paths are highlighted: the reversed motion of the jets causes the induction of opposite currents in the two halves of the duct which, to satisfy the charge conservation, form 4 loops with a saddle point in the duct center.

Since viscous and inertia effects are negligible in the core region, the electromagnetic and buoyancy forces balance each other and it is found that the component $j_x = O(1)$ is a linear function $j_x = -x$. From (5) and (6), it is obtained that $j_y = y$ and $\phi = \phi_H(x) + (1/2)(1 - y^2)$, where the potential of the Hartmann wall can be expressed as $\phi_H = 1/2 \ (1/M + c_H)^{-1}x^2$ [12].

For perfectly conducting walls, the Hartmann wall potential is zero and then the potential in the core region is constant in the direction perpendicular to the magnetic field. This result can be clearly observed in Figure 3b along with the parabolic profile characteristic of the field lines direction. From the Ohm's law (5) it can be found that the only non-zero component of the velocity in the core is the axial one, which it can be written as

$$w = -\partial_x\phi - j_x = [(1/M + c_H)^{-1} + 1]x \tag{12}$$

The velocity is therefore linear and independent by the Hartmann number. If the potential at the side wall is called ϕ_S, it is obvious that $\phi_S = \phi_H = 0$ and then a proper side layer solution has to be found in order to match with the core plateau. The result is a steep potential gradient which acts as an electromagnetic pump, driving the fluid from the strong dampening region of the core to the side layer, and forms a jet [3]. Velocity profiles for increasing value of M are provided in Figure 4 where it can be observed as the peak velocity scales with $M^{1/2}$.
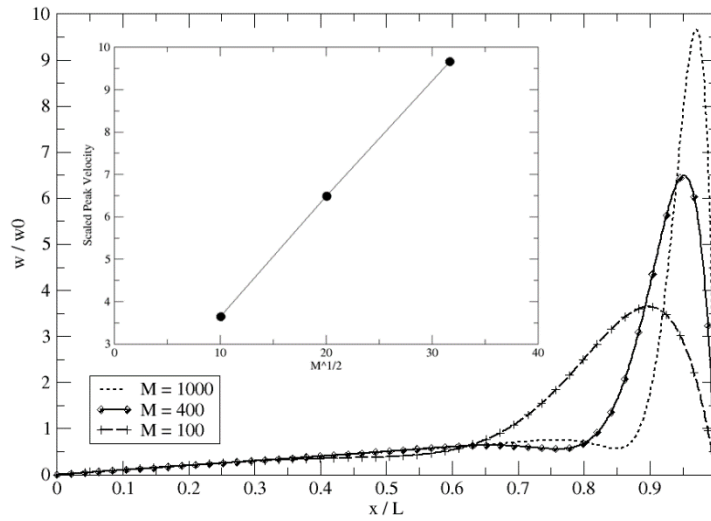
Figure 4 Side wall velocity profile for $c = \infty$ and increasing M. On the diagram, w_{MAX} is plotted against $M^{1/2}$

4.2. Perfectly insulating walls

If the case of perfectly insulating duct ($c = 0$) is considered, the currents close through the boundary layer (Figure 5b). A gradient $\partial_x \phi_H = O(M)$ will appear in the core region alongside with a parabolic potential profile (Figure 5a). The Hartmann number term will dominate in (12) and the core velocity takes the form $w \cong Mx$.
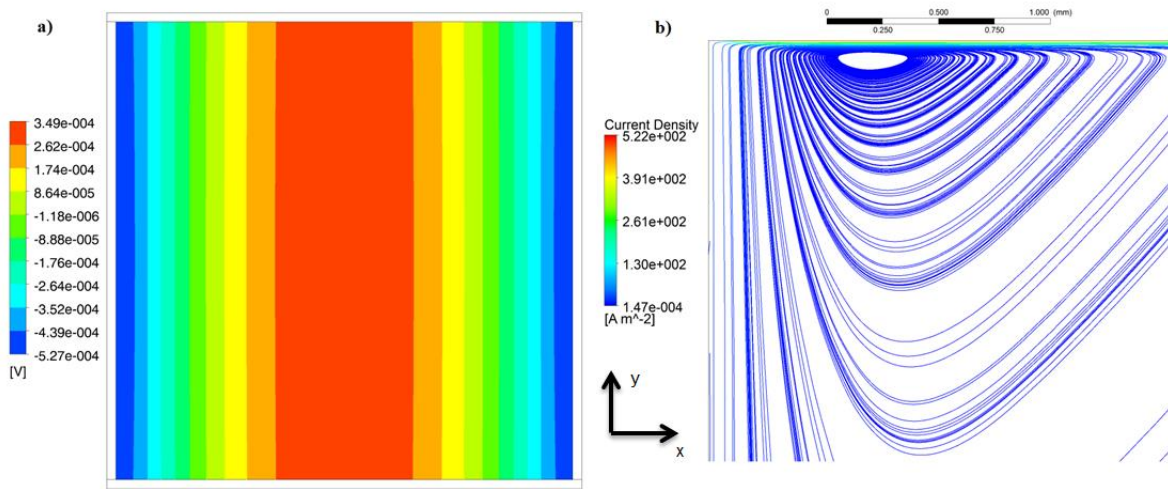

Figure 5 a) Electric potential contour for $c = 0$ (left), **b)** Current closure through the Hartmann boundary layer (right)

In Figure 6a the side wall profile for $c = 0$ and increasing M is shown. For a wall of finite electric conductivity, the behavior of the flow would be included inside the variable space defined by the two limiting cases discussed. Starting from $c = \infty$, a decrease of the wall conductance ratio will force the current to gradually shunt from the wall to the boundary layer. This will cause a net decrease of the damping effect exerted by the Lorentz force in the side layer, due to the more resistive path and the turning of the currents toward the magnetic field direction. The formation of stronger jets due to the intense electromagnetic drag still present in the core is promoted. When $c \to 0$, the flow rate tends to normalize with the fluid flowing back into the core from the side layers thanks to the decrease of the MHD damping (Figure 6b).
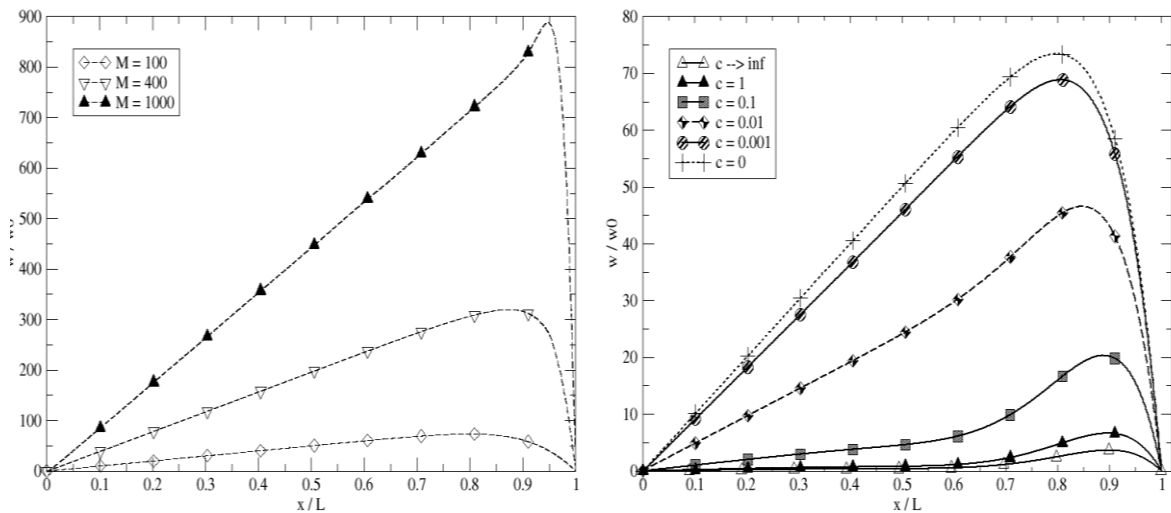
Figure 6 a) Side wall velocity profile for $c = 0$ and increasing M (left)**, b)** Side wall velocity profile for c ranging from 0 to ∞ and $M = 100$ (right)
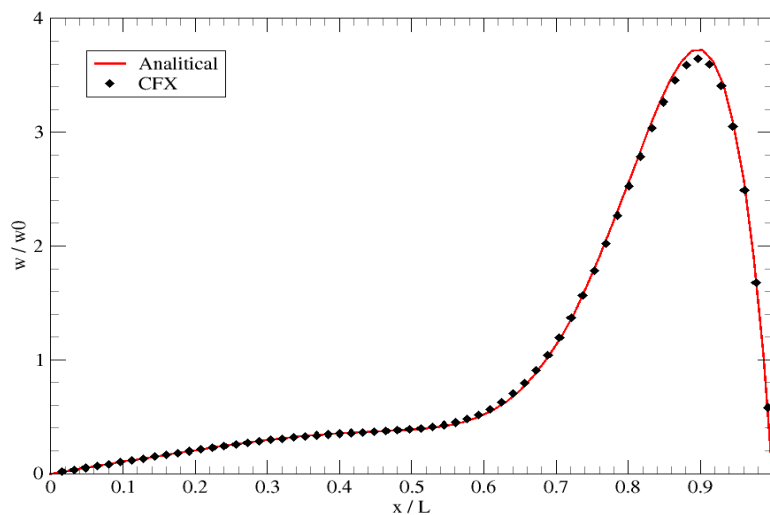
Figure 7 Validation of numerical results for the $c = \infty$, $M = 100$ test case

4.3. Validation results

ANSYS-CFX was able to represent correctly all the features described for every value of conductance ratio and Hartmann number. In the Figures 7, 8a and 8b; a comparison between the numerical results produced by the code and the analytical solution is provided. Although good quality results were produced in every test case, as it can be seen in Table 2, a slowing convergence rate was observed for high values of the Hartmann number due to the stronger coupling between the velocity and the magnetic field. Moreover, this issue was worsened when a low value of the conductance ratio was also considered, since the closure of the currents through the boundary layer requires the use of more resources than those needed for perfectly conducting walls.
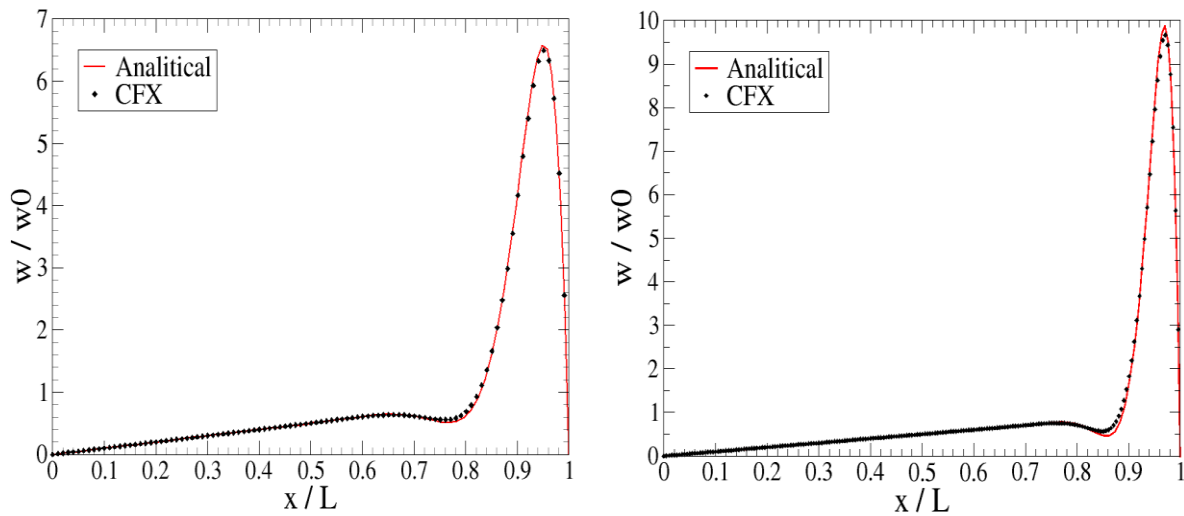
Figura 8 a) Validation of numerical results for the $c = \infty$, $M = 400$ test case (left), **b)** validation of numerical results for the $c = \infty$, $M = 1000$ test case (right)

5. Conclusions

In this paper a numerical study of the buoyant flow in a vertical square duct with differentially heated walls and a transversal magnetic field applied has been presented. The code ANSYS© CFX-15 was employed to perform the simulations, thanks to its MHD add-on. A description of the reference flow

Table 2 Overview of validation indices

Test Case		Peak Error [%]	Integral Error [%]
M	c		
100	0	0.68	-
	∞	2.01	0.79
400	0	4.08	-
	∞	1.26	1.49
1000	0	2.08	-
	∞	2.20	1.46

was provided for values of the conductance ratio ranging from 0 to ∞ and for *M* ranging from 10^2 to 10^3. The code was able to reproduce the features described in regard of electric potential, Lorentz force, current paths and velocity profile. The quality of the numerical results was assessed employing two indices, a local error and an integral error, and it was found in excellent agreement both with theoretical solutions in [2] and previous calculations presented in [8] and [12]. Although not included in this paper, analogous simulations for the benchmark of pressure-driven laminar flows have been performed which showed the same degree of accuracy [13].

Slower convergence was observed for high value of *M* and low conductivity walls and for $M > 10^3$, cases not presented here: severe oscillations of the residuals also occurred in these cases. Particular attention should be paid in the realization of the computational grid and in the choosing of the solver options in order to produce good quality results.

Nevertheless, ANSYS© CFX-15 can be considered as a reliable tool to perform analyses for 2D MHD buoyant flows. Further validation studies are needed in order to assess the behavior of the code in more complex geometries and 3D MHD flows, a necessary condition to satisfy in order for a code to being deemed useful in aiding the design of tokamak fusion reactors blankets.

List of symbols

Physical quantities

b	Channel half-width in x-direction
B	Magnetic induction [T]
g	Gravitational acceleration [m s^{-2}]
j	Current density [A m^{-2}]
l	Channel half-width in y-direction
L	Characteristic length [m]
p	Pressure [Pa]
Q	Heat source
T	Temperature [K]
v	Velocity [m s^{-1}]

Greek symbols

β	Thermal expansion coefficient [K^{-1}]
δ	Boundary layer thickness
ν	Kinematic viscosity [m^2 s^{-1}]
ρ	Density [kg m^{-3}]
σ	Electrical conductivity [S m^{-1}]
ϕ	Electric potential [V]

Dimensionless parameters

Gr	Grashof number
M	Hartmann number
Pe	Péclet number
Pr	Prandtl number
Re	Reynolds number
R_m	Magnetic Reynolds number
c	Wall conductance ratio

Acronyms and abbreviations

MHD	Magneto-hydrodynamics
CFD	Computational fluid-dynamics
LiPb	Lithium-lead eutectic alloy
PPPT	Power Plant Physics & Technology

References

[1] Smolentsev S, Moreau R, Bühler L and Mistrangelo C, 2010 MHD thermofluid issues of liquid-metal blankets: phenomena and advances *Fusion Eng. Des.* **85** 1196-1205

[2] Bülher L, 1997 Laminar buoyant magnetohydrodynamic flow in vertical rectangular ducts *Phys. Fluids* **10** 223-236

[3] Tagawa T, Authié G and Moreau R, 2002 *Eur. J. Mech. B-fluids* **21** 383-398

[4] Aleksandrova S and Molokov S, 2004 *Fluid Dyn. Res.* **35** 37-66

[5] Authié G, Tagawa T and Moreau R, 2003 *Eur. J. Mech. B-fluids* **22** 203-220

[6] Burr U, Barleon L, Jochmann P and Tsinober A, 2003 Magnetohydrodynamic convection in a vertical slot with horizontal magnetic field *J. Fluid Mech.* **475** 21-40

[7] Smolentsev S, Badia S, Bhattacharyay R and Bühler L, 2015 An approach to verification and validation of MHD codes for fusion applications *Fusion Eng. Des.* **100** 65-72

[8] Di Piazza I and Bühler L, 2000 *Fusion Technol.* **38** 180-189

[9] ANSYS© CFX., 15.0, CFX-Solver Theory Guide, 2013, ANSYS Inc.

[10] Davidson P A, 2001 *An Introduction to Magnetohydrodynamics* (Cambridge: Cambridge University Press)

[11] De les Valls E M, 2008 *J. Nucl. Mater.* **376(3)** 353-357

[12] Mistrangelo C and Bühler L, 2012 *IEEE T. Plasm Sci.* **40(3)** 584-589

[13] Tassone A, 2015 CFD simulation of the MHD flow in the WCLL breeding blanket module MSc final thesis (Università di Roma "La Sapienza", Rome, Italy).